International Journal of Heat and Mass Transfer 254 (2026) 127623

Contents lists available at ScienceDirect

International Journal of Heat and Mass Transfer

journal homepage: www.elsevier.com/locate/hmt

Wall roughness and viscous dissipation effects in microchannel heat sinks with semicircular cross-section

A. Barletta *, M. Celli, P.V. Brandão

Department of Industrial Engineering, Alma Mater Studiorum Università di Bologna, Viale Risorgimento 2, 40136 Bologna, Italy

ARTICLE INFO

Keywords:
Laminar flow
Forced convection
Microchannel
Semicircular duct
Surface roughness
Viscous dissipation

ABSTRACT

A statistical analysis of the wall roughness effect is carried out to determine the impact of the shape uncertainty on the Poiseuille number and Nusselt number of laminar forced convection. The focus is on the fully developed regime in a semicircular microchannel where the heat transfer occurs from the diametrical plane boundary, modelled as a perfectly smooth surface. On the other hand, the curved semicircular boundary is devised as rough and with a negligible wall heat flux. Three types of thermal boundary conditions are implemented: the T condition, the H1 condition and the H2 condition. The T condition serves to model a case where the fluid temperature does not undergo any change in the streamwise direction, while the H1 and H2 conditions are employed to describe a net heating of the fluid. A statistical sample of several different rough microchannels is used to detect the actual effects of roughness on the Poiseuille number and on the Nusselt number, through the evaluation of their average values and standard deviations. The governing local momentum and energy balance equations are solved numerically by a finite element method taking into account the viscous dissipation contribution to the local energy balance.

1. Introduction

The use of microchannels is fundamental in modern thermal management systems, especially in applications requiring compact and efficient heat removal such as microelectronics, microreactors, and biomedical devices [1–7]. Microchannels are typically characterized by hydraulic diameters usually less than 100 μm. When a fluid is actively driven through these internal passages with a pressure gradient supplied by external pumping, the resulting convective heat transfer takes place in a forced convection regime. Due to the high area-to-volume ratio of microchannels, they enable efficient heat exchange even with relatively low flow rates, making them ideal for miniaturized heat sinks [8–10].

In microchannels, the small scale of the flow passages introduces several complex physical phenomena that are either negligible or less significant in conventional-sized channels. Among the most critical of these are viscous dissipation and wall roughness, both of which can significantly affect the heat transfer and fluid flow behaviour [11–23].

Viscous dissipation is the irreversible conversion of mechanical energy into heat due to viscous friction within the fluid. In microchannels, where the flow velocities may be large relative to the small cross-sectional area, viscous heating effects are amplified. As a result, the fluid experiences a significant temperature rise due to internal friction. The presence of viscous dissipation adds a source term to the energy equation which can lead to increased fluid temperatures, altering the temperature gradient between the wall and the fluid, and thus impacting the overall heat transfer rate [15,24].

No real microchannel has perfectly smooth walls. Surface roughness due to manufacturing tolerances, etching artifacts or deliberate texturing alters both hydrodynamic and thermal behaviour. At the microscale, a roughness element of just a few microns can occupy a significant fraction of the channel's hydraulic diameter. Thus, unlike in conventional systems, where wall roughness may be treated as a minor perturbation, in microchannels, even small-scale surface irregularities can have a disproportionately large influence on the flow and heat transfer characteristics. Manufacturing techniques such as micromachining, etching, or 3D printing can introduce surface imperfections that disturb the fully-developed laminar flow profile typically expected in smooth microchannels. Roughness may cause an increase in the friction factor, leading to a higher pressure drop for a given flow rate. From a heat transfer standpoint, roughness may enhance heat transfer due to an increased fluid-to-solid exchange area or it can even induce a decrease in the heat transfer rate due to the flow velocity reduction in the near-wall region [16,18,20,25].

Forced convection in microchannels is highly sensitive to effects that are often negligible in macroscale systems. Viscous dissipation introduces additional heating, affecting temperature distributions and

* Corresponding author.
E-mail address: antonio.barletta@unibo.it (A. Barletta).

https://doi.org/10.1016/j.ijheatmasstransfer.2025.127623
Received 30 May 2025; Received in revised form 14 July 2025; Accepted 28 July 2025
Available online 21 August 2025
0017-9310/© 2025 The Authors. Published by Elsevier Ltd. This is an open access article under the CC BY license (http://creativecommons.org/licenses/by/4.0/).

potentially reducing thermal control accuracy. Wall roughness modifies flow characteristics and can either enhance or contrast heat transfer depending on the roughness geometry and flow conditions. Accurate modelling of microchannel systems must consider these phenomena to ensure optimal design and operation in high-performance thermal applications.

Viscous dissipation and wall roughness interact: rougher surfaces elevate shear rates locally, further amplifying viscous heating [26,27]. Consequently, optimization of microchannel heat sinks involves a careful balancing act. Computational fluid dynamics (CFD) simulations and micro-PIV (particle image velocimetry) experiments help map out the parameter space of Reynolds number, Brinkman number and roughness geometry. Material selection, fabrication method (*e.g.*, plasma-based DRIE, micromilling, 3D printing) and coolant properties are chosen to minimize detrimental effects while maximizing heat transfer density. In many applications, a moderate, controlled roughness pattern, such as staggered micro-rib arrays, provides enough mixing to enhance thermal performance without incurring prohibitive pressure drops. At the same time, low-viscosity, high-thermal-conductivity fluids (e.g., water–glycol mixtures or nanofluids) are preferred to control the effects of viscous dissipation.

The aim of this paper is the analysis of the mechanical and thermal characteristics of the forced convection flow across an array of semicircular microchannels employed to cool a heated polished metal plate. Such a simplified heat sink design is meant to better understand the actual heat transfer process involved in the cooling of an electronic circuit board. The basic scheme is reported in Fig. 1. We assume an array of parallel microchannels etched on the surface of a solid layer. By sealing the layer on the heated metal plate, we devise a heat sink system where the thermal energy from the metal plate is convected away through the microchannels. We also assume that the thermal characteristics of the heat sink can be consistently inferred from the behaviour of a single microchannel, meaning that the thermal interaction between neighbouring microchannels is considered as negligible. The plane diametrical boundary of each microchannel is heated and the heating is modelled through either a H1 or a H2 boundary condition, consistently with the definitions given by Shah and London [28]. A special case of the H1 boundary condition, *i.e.* the T boundary condition, is also studied for the sake of completeness as it represents the case where the diametrical boundary is isothermal both in the perimetral and in the streamwise directions. The analysis of the special T boundary condition shows up an independence from the Brinkman number or, in other terms, the Brinkman number is fixed to a geometry-dependent value, Br_{T}. Compared to the heat flux supplied through the diametrical boundary, the semicircular boundary heat flux is considerably smaller so that, in this analysis, such a boundary is considered as thermally insulated. A further internal source of fluid heating is viscous dissipation, namely the mechanical work to heat conversion due to the forced flow in the microchannel. Such an effect, which may be significant especially in the small scale typical of microfluidics [15] is parametrized by the Brinkman number, Br. Surface roughness along the semicircular boundary is described by the dimensionless parameter γ, defined as the maximum ratio between the length of the surface spikes to the semicircle radius. The computational approach to the surface roughness effects is grounded on a statistical scheme by considering, in each case, a population of 500 randomly generated deformations of the semicircle. Each deformed path is a polygonal connecting 45 points, defined within the tolerance introduced by the roughness parameter γ.

This study develops the ideas recently discussed in the case of circular microducts by Barletta et al. [26] and Sphaier et al. [27]. In particular, the approach where the roughness effect is examined on a statistical basis by simulating numerically the forced convection flow in randomly generated cross-sectional geometries is here applied to the case of semicircular microchannels. In Section 2, with reference to a single microchannel, the physical assumptions underlying our analysis and the mathematical model adopted are described in details. In Section 3, the nondimensional analysis of the model developed is carried showing up the main dimensionless parameters governing the flow and the heat transfer process, providing also a description of the finite-element solver procedure employed for the numerical analysis of the mathematical model. Section 4 is devoted to the analysis of the smooth semicircular duct, namely the special case where the surface roughness is considered as negligible. This special case is also employed as a test for the assessment of the numerical solver accuracy. The effects of the wall roughness and its interplay with the viscous dissipation effect are drawn in Section 5.

Nomenclature

a	constant temperature gradient
Br	Brinkman number
c	specific heat
k	thermal conductivity
n	integer
$\hat{\mathbf{n}}$	unit normal vector
N	number of nodes along the polygonal
Nu	Nusselt number
p	pressure
$\mathcal{P}$	cross-sectional perimeter
$\mathcal{P}_1, \mathcal{P}_2$	nominally semicircular boundary, diametrical boundary
Po	Poiseuille number
q_w	average wall heat flux
r	radial coordinate
r_h	nominal hydraulic radius of the smooth semicircular duct
r_0	radius of the semicircle
$\mathcal{S}$	cross-sectional area
T	temperature
T_b	bulk temperature
T_w	average wall temperature
u	velocity
u_0	reference velocity
u_m	mean flow velocity
x, y, z	Cartesian coordinates
x_n, y_n	coordinates of the polygonal points
Greek symbols	
α	thermal diffusivity
γ	roughness dimensionless parameter
$\delta r_n, \theta_n$	radius uncertainty, angular position of the nth polygonal point
μ	dynamic viscosity
ν	kinematic viscosity
σ	dimensionless streamwise temperature gradient
Subscripts, superscripts	
*	dimensionless quantity
T, H1, H2	thermal boundary conditions

2. Mathematical model

Let us consider a microchannel with a semicircular cross-section heated through its diametrical boundary side (see Fig. 2). On the other hand, the semicircular boundary side is assumed to be adiabatic, meaning that the main heat transfer mechanism is the forced convection taking place in the axial z direction. This simplifying assumption is realistic especially when the microchannel is obtained by etching a solid layer with poor thermal conductivity and/or with a thickness much larger than the microchannel diameter. The diametrical side is the contact surface with a heated metal plate. Depending on the fabrication characteristics of microchannels, we assume that the semicircular side

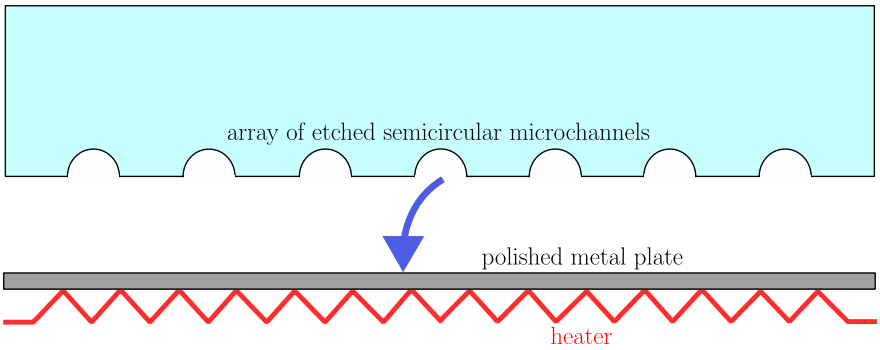

Fig. 1. Cross-sectional view of an array of semicircular microchannels employed to cool a heated plate.

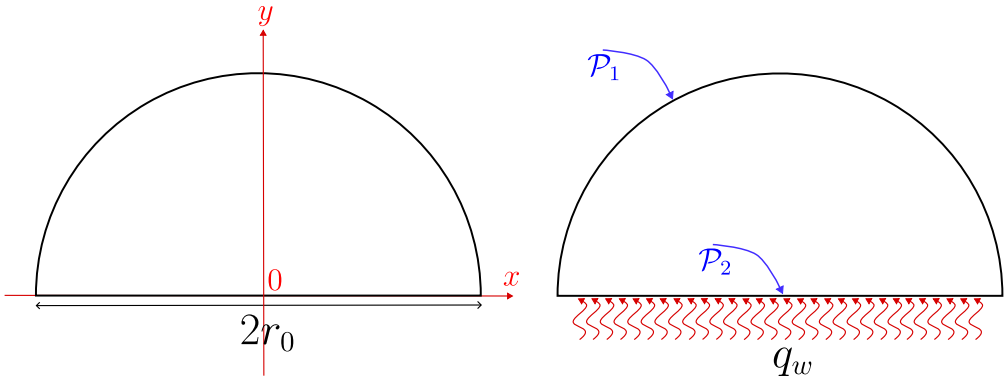

Fig. 2. Sketch of the microchannel nominal cross-section.

is endowed with a roughness significantly larger than that of the heated metal plate, so that the latter will be modelled as perfectly smooth throughout this study. The nominal radius of the semicircular region is r_0. The semicircular region lies in the xy plane, while the z axis is parallel to the streamwise direction.

The surface roughness of the microchannel curved boundary is modelled by assuming a random change of the semicircle to a polygonal path, $\mathcal{P}$, with N nodes having positions (x_n, y_n) given by

$$\begin{aligned} &x_1 = r_0, \quad y_1 = 0, \\ &x_n = (r_0 + \delta r_n)\cos\theta_n, \quad y_n = (r_0 + \delta r_n)\sin\theta_n, \qquad \text{for} \quad n = 2, \ \dots \ , N-1, \\ &x_N = -r_0, \quad y_N = 0, \end{aligned} \tag{1}$$

where δr_n and θ_n are random variables within the ranges

$$-\gamma r_0 \le \delta r_n \le \gamma r_0, \quad \frac{(n-2)\pi}{N-2} < \theta_n < \frac{(n-1)\pi}{N-2}. \tag{2}$$

The dimensionless parameter γ employed in Eq. (2) is a measure of the roughness size relative to the nominal radius r_0. Eq. (2) provides the definition of the roughness parameter γ as the maximum allowed value for $|\delta r_n|/r_0$.

The polygonal path $\mathcal{P}$ is closed by joining the points (x_N, y_N) and (x_1, y_1) with the straight diametrical line. Thus, the closed polygonal path $\mathcal{P}$ is the boundary of the rough microchannel cross-section, denoted as $\mathcal{S}$. A sample region $\mathcal{S}$ obtained with $N = 45$ and $\gamma = 0.02$ is shown in Fig. 3(a).

Throughout our analysis, the generation algorithm for the roughness nodes (x_n, y_n) relies on the implicit assumption of a uniform statistical distribution. In fact, the implementation is based on a pseudorandom number generation for the polar coordinates of the nodes. Different statistical assumptions could have been made, *e.g.* a Gaussian distribution, but there is no evidence that such assumptions may lead to more realistic models. In the absence of any further information, a uniform statistical distribution of data is to be preferred to avoid the introduction of any extra bias in the results.

The flow in the streamwise direction is stationary, incompressible and fully developed. Thus, the velocity field $\mathbf{u}$ has just one nonzero component, *i.e.*, that along the z axis, denoted as u. As a consequence of the local mass balance equation, $\boldsymbol{\nabla}\cdot\mathbf{u} = 0$, such a velocity component is independent of z. Hence, the average velocity across the microchannel is a constant denoted as u_m.

The governing equations for the fully developed flow (both hydrodynamically and thermally developed flow) are the local momentum balance and the local energy balance equations written as

$$\begin{aligned} &\nabla^2 u = \frac{1}{\mu}\frac{\mathrm{d}p}{\mathrm{d}z}, \\ &u\,\frac{\partial T}{\partial z} = \alpha\,\nabla^2 T + \frac{\nu}{c}\,|\boldsymbol{\nabla} u|^2, \end{aligned} \tag{3}$$

where $\mathrm{d}p/\mathrm{d}z$ is the constant pressure gradient driving the flow, μ is the dynamic viscosity, ν is the kinematic viscosity, α is the thermal diffusivity of the fluid and c is its specific heat, while T is the temperature field. The Laplacian ∇^2 operator and the gradient $\boldsymbol{\nabla}$ operator are intended as 2-dimensional in the xy plane. Indeed, the fully developed regime implies that $\partial T/\partial z$ is a constant, hereafter denoted as a. As a consequence, we can write

$$\begin{aligned} &\frac{\partial T}{\partial z} = \frac{\mathrm{d}T_b}{\mathrm{d}z} = a, \\ &\text{for} \quad T_b = \frac{1}{S u_m}\iint_{\mathcal{S}} T(x,y,z)u(x,y)\,\mathrm{d}x\,\mathrm{d}y, \quad u_m = \frac{1}{S}\iint_{\mathcal{S}} u(x,y)\,\mathrm{d}x\,\mathrm{d}y, \end{aligned} \tag{4}$$

with T_b the bulk temperature. We emphasize that the term $\nu\,|\boldsymbol{\nabla} u|^2/c$ in the second Eq. (3) represents the viscous dissipation contribution to the local energy balance.

For the sake of simplicity, we will always employ the same symbols $\mathcal{P}$ and $\mathcal{S}$ to denote both the geometrical objects and their measures (perimeter and area, respectively). The solution of the first Eq. (3) with

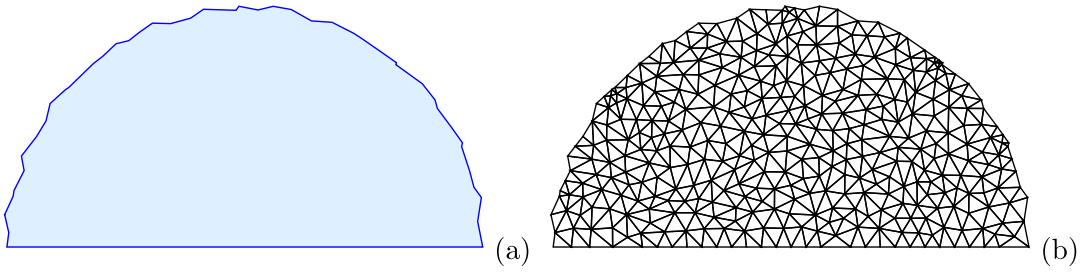

Fig. 3. A typical domain S (a), obtained with $N = 45$ and $\gamma = 0.02$, and one of its possible unstructured meshes (b) for the finite-element solver.

the no-slip boundary conditions

$$u = 0, \quad (x, y) \in \mathcal{P}, \tag{5}$$

yields the velocity profile $u(x, y)$ and, by employing Eq. (4), the average velocity u_m. After having determined $u(x, y)$, the second Eq. (3) leads to the determination of $T(x, y, z)$. The solution process of the second Eq. (3) requires the statement of boundary conditions at the rough semicircular path, denoted as $\mathcal{P}_1$, and at the diametrical straight line, denoted as $\mathcal{P}_2$ (see Fig. 3). Obviously, $\mathcal{P} = \mathcal{P}_1 \cup \mathcal{P}_2$. While the boundary condition at $\mathcal{P}_1$ prescribes thermal insulation,

$$\hat{\mathbf{n}} \cdot \boldsymbol{\nabla} T = 0, \qquad \text{for} \quad (x, y) \in \mathcal{P}_1, \tag{6}$$

with $\hat{\mathbf{n}}$ the unit outward normal to $\mathcal{P}$, the thermal boundary condition at $\mathcal{P}_2$ can be formulated either as a H1 condition or as a H2 condition, where both are meant to describe a wall heating process,

$$\begin{aligned} &\text{H1 condition:} \quad \frac{\partial T}{\partial x} = 0, \qquad \text{for} \quad -r_0 < x < r_0, \quad y = 0; \\ &\text{H2 condition:} \quad -k\frac{\partial T}{\partial y} = q_w = \text{uniform}, \qquad \text{for} \quad -r_0 < x < r_0, \quad y = 0, \end{aligned} \tag{7}$$

where k is the fluid thermal conductivity.

The two different statements of the wall heating conditions, given by Eq. (7), are those introduced and defined by Shah and London [28]. In particular, for the statement of the H1 boundary condition formulated in Eq. (7), $\partial T/\partial x = 0$ means that T is uniform along the x direction with $-r_0 < x < r_0$. In fact, the H1 condition prescribes a uniform temperature of the heated side along the perimetrical direction (in this case, the x axis), while T, in general, changes in the streamwise direction (in this case, the z axis) with a slope $\partial T/\partial z$ dependent on the wall heat flux q_w and the viscous dissipation rate.

There are useful definitions of the average temperature of the heated boundary $\mathcal{P}_2$ and the average wall heat flux at $\mathcal{P}_2$,

$$T_w = \frac{1}{2r_0}\int_{-r_0}^{r_0} T(x, 0, z)\,\mathrm{d}x, \quad q_w = -\frac{k}{2r_0}\int_{-r_0}^{r_0} \left.\frac{\partial T}{\partial y}\right|_{y=0} \mathrm{d}x. \tag{8}$$

The difference between the boundary conditions H1 and H2 is that, in the former case, the temperature T is uniform and equal to T_w at every point in $\mathcal{P}_2$. On the other hand, with the condition H2, the normal derivative $\partial T/\partial y$ is uniform over $\mathcal{P}_2$ and equal to $-q_w/k$. Both H1 and H2 wall heating conditions result in a nonzero value of the constant a, defined by Eq. (4). Useful dimensionless parameters are the Poiseuille number and the Nusselt number defined as

$$\mathrm{Po} = \frac{u_0}{u_m}, \quad \mathrm{Nu} = \frac{2r_h q_w}{k(T_w - T_b)}, \qquad \text{for} \quad u_0 = -\frac{2r_h^2}{\mu}\frac{\mathrm{d}p}{\mathrm{d}z}, \tag{9}$$

where r_h is the nominal hydraulic radius which, for a semicircular cross-section with radius r_0, is given by

$$r_h = \frac{\pi}{\pi + 2}\, r_0. \tag{10}$$

By employing Eqs. (4) and (8), one can prove that both Po and Nu are constants, *i.e.*, they are independent of z.

3. Nondimensional formulation

Let us define the dimensionless coordinates, operators and fields, denoted with asterisks,

$$(x^*, y^*) = \frac{(x, y)}{r_h}, \quad \boldsymbol{\nabla}^* = r_h \boldsymbol{\nabla}, \quad \nabla^{*2} = r_h^2 \nabla^2, \quad u^* = \frac{u}{u_0}, \quad T^* = k\,\frac{T - T_w}{q_w r_h}, \tag{11}$$

as well as the Brinkman number and the dimensionless streamwise temperature gradient,

$$\mathrm{Br} = \frac{\mu\, u_m^2}{2 r_h q_w}, \quad \sigma = \frac{k r_h u_m a}{\alpha\, q_w}. \tag{12}$$

The Brinkman number determines the strength of the viscous dissipation effect. Using Eqs. (4), (11) and (12), the governing Eqs. (3) can be rewritten as

$$\begin{aligned} &\nabla^{*2} u^* + \frac{1}{2} = 0, \\ &\nabla^{*2} T^* - \mathrm{Po}\,\sigma u^* + 2\,\mathrm{Po}^2\mathrm{Br}\,|\boldsymbol{\nabla}^* u^*|^2 = 0. \end{aligned} \tag{13}$$

The nondimensional boundary conditions (5)–(7) are given by

$$\begin{aligned} &u^* = 0, \qquad \text{for} \quad (x^*, y^*) \in \mathcal{P}^*, \\ &\hat{\mathbf{n}} \cdot \boldsymbol{\nabla}^* T^* = 0, \qquad \text{for} \quad (x^*, y^*) \in \mathcal{P}_1^*, \\ &\text{H1 condition:} \quad T^* = 0, \qquad \text{for} \quad -\frac{\pi + 2}{\pi} < x^* < \frac{\pi + 2}{\pi}, \quad y^* = 0; \\ &\text{H2 condition:} \quad \frac{\partial T^*}{\partial y^*} = -1, \qquad \text{for} \quad -\frac{\pi + 2}{\pi} < x^* < \frac{\pi + 2}{\pi}, \quad y^* = 0. \end{aligned} \tag{14}$$

In fact, we denote with $\mathcal{S}^*$, $\mathcal{P}^*$ and $\mathcal{P}_1^*$ the nondimensional objects obtained by scaling the coordinates (x, y) as defined by Eq. (11). In Eq. (14), the H1 condition is reformulated by taking into account that T is uniform over the diametrical side $\mathcal{P}_2$, so that $T = T_w$ at every point on that boundary.

On account of Eqs. (4), (9) and (11), one can evaluate Po and Nu as

$$\mathrm{Po} = \frac{\mathcal{S}^*}{\displaystyle\iint_{\mathcal{S}^*} u^*(x^*, y^*)\,\mathrm{d}x^*\,\mathrm{d}y^*}, \quad \mathrm{Nu} = -\frac{2\mathcal{S}^*}{\mathrm{Po}\displaystyle\iint_{\mathcal{S}^*} T^*(x^*, y^*)\,u^*(x^*, y^*)\,\mathrm{d}x^*\,\mathrm{d}y^*}. \tag{15}$$

As explicitly specified in Eq. (15), T^* is independent of z^*. This is a consequence of Eq. (11), as well as of Eqs. (4) and (8) which imply that $\partial T/\partial z = a = \mathrm{d}T_w/\mathrm{d}z$.

By integrating the second Eq. (13) over $\mathcal{S}^*$, by employing Gauss–Green theorem and by employing Eqs. (4), (8) and (11), one obtains an expression for σ, namely

$$\sigma = \frac{2(\pi + 2)}{\pi\,\mathcal{S}^*} + \frac{2\mathrm{Po}^2\mathrm{Br}}{\mathcal{S}^*}\iint_{\mathcal{S}^*} |\boldsymbol{\nabla}^* u^*(x^*, y^*)|^2\,\mathrm{d}x^*\,\mathrm{d}y^* = \frac{2(\pi + 2)}{\pi\,\mathcal{S}^*} + \mathrm{Po}\,\mathrm{Br}, \tag{16}$$

where the evaluation of the double integral has been carried out by multiplying the first Eq. (13) by u^*, integrating by parts the resulting

Table 1
Test of the numerical finite-element solver: evaluation of Po with $\gamma \to 0$ and different mesh refinements (MaxCellMeasure) and the absolute value of the relative error with respect to the exact result given by Eq. (18).

MaxCellMeasure	Po	|relative error| (%)
10^{-1}	15.7686	0.011
$10^{-1.5}$	15.7672	0.0024
10^{-2}	15.7669	0.00039
$10^{-2.5}$	15.7668	0.000030
10^{-3}	15.7668	4.0×10^{-6}
$10^{-3.5}$	15.7668	5.3×10^{-7}
10^{-4}	15.7668	1.4×10^{-8}

equation and then by employing the no-slip conditions together with Eq. (15). One may mention that a special case of the H1 condition is when $\sigma = 0$. This is a case such that the boundary temperature is not only uniform along the diametrical line $\mathcal{P}_2$, but also in the streamwise direction z. This special case defines the so-called T condition, identified through a special value of Br, given by

$$\mathrm{Br}_\mathrm{T} = -\frac{2(\pi+2)}{\pi\,\mathrm{Po}\,\mathcal{S}^*}. \tag{17}$$

We mostly relied on the classical taxonomy of boundary conditions proposed by Shah and London [28], with the H1 and H2 conditions being the main candidates to the modelling of uniform wall heating. The difference between them relies on the former being more suitable for walls with a high thermal conductivity, while the latter is more suitable for low thermal conductivity materials with a uniform wall thickness over the cross-section perimeter [28]. Given that H1 and H2 conditions are idealizations, a real case of uniform heating typically lies in between them and this justifies why discussing both these boundary conditions. The interest in the T condition is only lateral to the study presented in this paper, as the T condition is a notable special case of H1 condition which addresses a case of uniform cooling (one needs to remove heat from the duct boundary in order to prevent viscous dissipation from increasing the fluid temperature along the streamwise direction). Therefore, we consider the analysis of the T condition as a by-product of our analysis which comes out with no extra effort, while its interest for the applications is definitely minor.

The solution of Eqs. (13) and (14), as well as the evaluation of Po and Nu based on Eq. (15), can be obtained numerically by employing the finite-element PDE solver available in *Wolfram 14* [29]. The meshes employed for the solution process are unstructured, with triangular elements, and their generation is made through the built-in function ToElementMesh. The refinement of the meshes employed is controlled via the parameter MaxCellMeasure whose value defines the maximum area of the grid cells. Then, the numerical solution is developed by using the function NDSolveValue, while the double integrals needed to compute Po and Nu are evaluated through function NIntegrate. Fig. 3(b) shows a typical unstructured mesh for the sample domain $\mathcal{S}$ drawn in Fig. 3(a) for $N = 45$ and $\gamma = 0.02$.

4. The perfectly smooth semicircular duct

An important benchmark case is when the surface roughness tends to zero ($\gamma \to 0$) [28,30–34]. In this case, there exists an analytical expression of Po available in the literature [31,34],

$$\mathrm{Po} = \frac{8\pi^4}{(\pi+2)^2(\pi^2-8)} \approx 15.7668. \tag{18}$$

This exact result is used to test the convergence of the numerical solver by defining meshes with a decreasing value of the parameter MaxCellMeasure. The results of this test are reported in Table 1. This table shows that an excellent agreement within the first six significant figures is already attained with MaxCellMeasure $\to 10^{-2.5}$. Hereafter, all the computations for the microchannels with a rough or smooth boundary will be carried out with MaxCellMeasure $\to 10^{-3}$.

Table 2
Values of $\mathrm{Nu}_{\mathrm{H1}}$ and $\mathrm{Nu}_{\mathrm{H2}}$ with $\gamma \to 0$ for different Brinkman numbers.

Br	$\mathrm{Nu}_{\mathrm{H1}}$	$\mathrm{Nu}_{\mathrm{H2}}$
0	3.28168	3.17683
0.01	3.17278	3.07468
0.1	2.44317	2.38458
0.5	1.20826	1.19376
1	0.740440	0.734967
1.5	0.533771	0.530922
2	0.417297	0.415553
2.5	0.342549	0.341373
3	0.290512	0.289666
3.5	0.252200	0.251562
4	0.222815	0.222317
4.5	0.199563	0.199164
5	0.180706	0.180378

In the case where $\gamma \to 0$, we have

$$\mathcal{S}^* = \frac{(\pi+2)^2}{2\pi}, \quad \sigma = \frac{4}{\pi+2} + \frac{8\pi^4\,\mathrm{Br}}{(\pi+2)^2(\pi^2-8)}, \quad \mathrm{Br}_\mathrm{T} = -\frac{(\pi+2)(\pi^2-8)}{2\pi^4}, \tag{19}$$

where the expressions of σ and Br_T have been obtained by using Eqs. (16)–(18). On the other hand, the values of Nu for the cases H1 and H2 are obtained for prescribed values of Br. Except for the T condition where $\mathrm{Br} = \mathrm{Br}_\mathrm{T}$, we will consider only non-negative values of Br as the scope of our analysis is the case of a heated diametrical boundary.

The values of Nu can be determined numerically for the T boundary condition, as well as for the H1 and H2 boundary conditions with fixed values of Br. The value of Nu_T is

$$\mathrm{Nu}_\mathrm{T} = 3.95071, \tag{20}$$

while values of $\mathrm{Nu}_{\mathrm{H1}}$ and $\mathrm{Nu}_{\mathrm{H2}}$ are reported in Table 2 for some Brinkman numbers. An evident feature of these data is that $\mathrm{Nu}_{\mathrm{H1}}$ is greater than $\mathrm{Nu}_{\mathrm{H2}}$ as typical of fully developed forced convection in ducts [28]. However, the relative discrepancy is always small and it decreases with $\mathrm{Br} > 0$ being around 3.3%, at its largest, when $\mathrm{Br} = 0$. The effect of viscous dissipation, for conditions of uniform wall heating, tends to induce a continuous decrease in the value of Nu as Br increases. This behaviour reflects the trend of Nu versus Br whatever is the cross-sectional shape of the duct [28]. The data reported in Table 2 show that, as Br increases, Nu may become smaller than 1. Eventually, it tends to 0 when $\mathrm{Br} \to \infty$, in agreement with the trends shown for other cross-sectional geometries [28]. The physical argument underlying this behaviour can be described through the following steps:

- the heat transfer rate is given by $q_w/(T_w - T_b)$;
- with H1 and H2 boundary conditions, the wall heat flux q_w is prescribed;
- the difference $T_w - T_b$ gradually increases when the effect of viscous dissipation becomes more and more intense.

5. Discussion of the effects of wall roughness

The gradual increase of the wall roughness is monitored by fixing values of γ within the range $0 < \gamma \leq 0.1$. For each value of γ, a population of 500 different cross-sections is generated by means of random polygonal paths defined through Eqs. (1) and (2). In every population, we evaluate the mean value and the standard deviation for the parameters Po, Nu_T, $\mathrm{Nu}_{\mathrm{H1}}$ and $\mathrm{Nu}_{\mathrm{H2}}$. The first two parameters Po and Nu_T are not affected by Br. This feature already emerged in the case of the smooth semicircular duct discussed in Section 4. In fact, it is a general feature valid for every γ as Po is determined only by solving

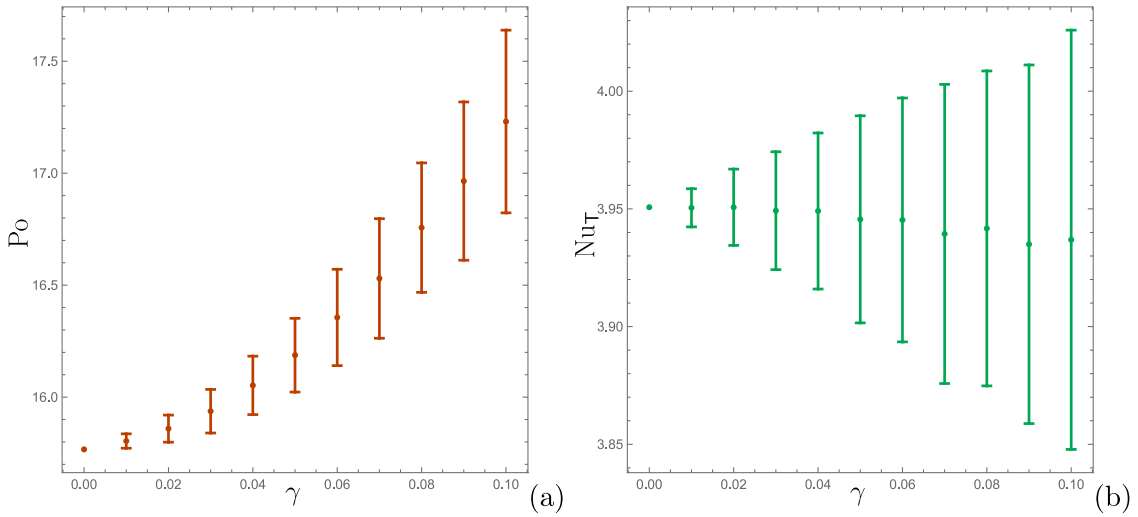

Fig. 4. Plots of Po (a) and Nu_T (b) versus γ. The dots indicate the mean value over the statistical population, while the segments show the uncertainties in a one standard deviation range from the mean value.

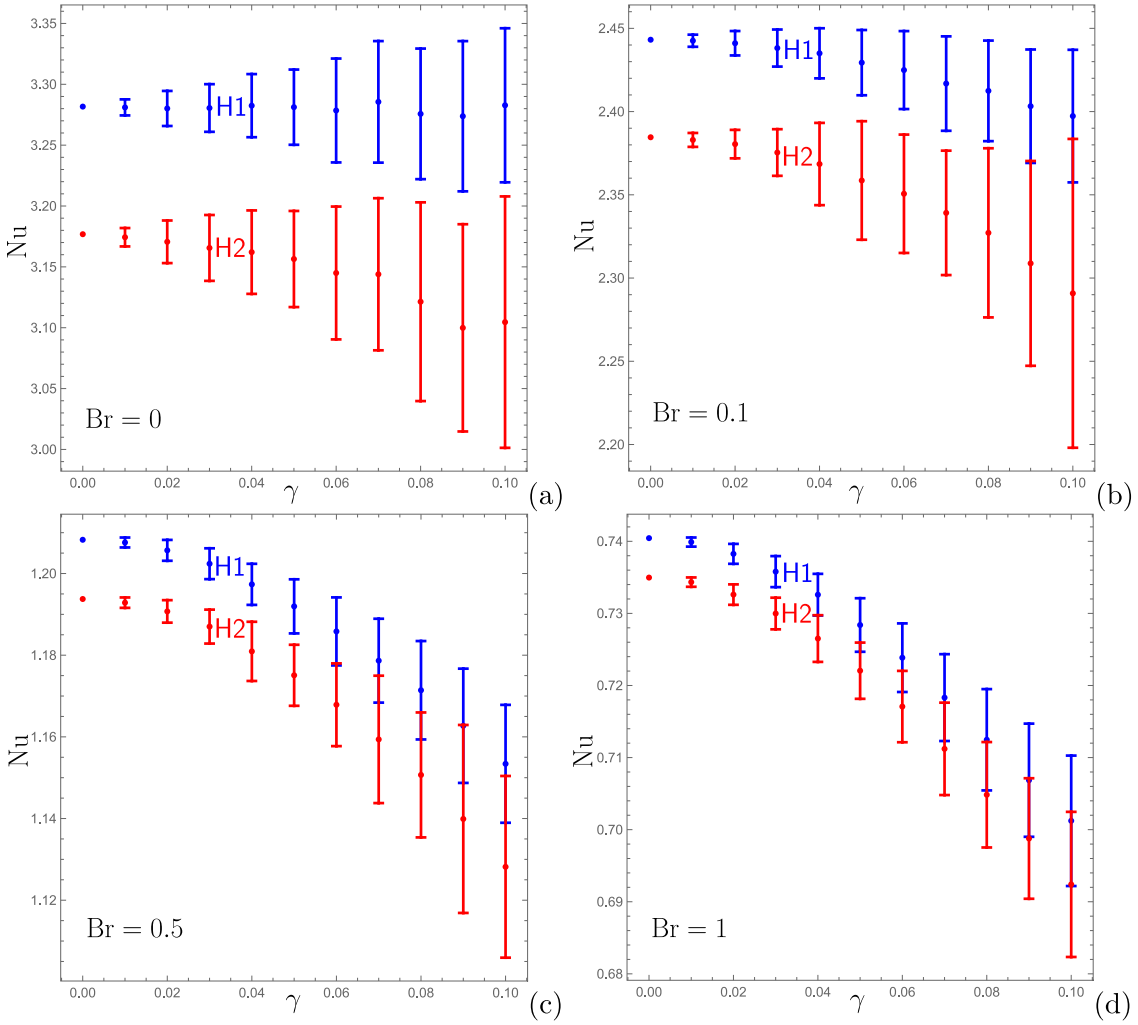

Fig. 5. Plots of Nu_{H1} (in blue) and Nu_{H2} (in red) versus γ for Br = 0 (a), Br = 0.1 (b), Br = 0.5 (c) and Br = 1 (d). The dots indicate the mean value over the statistical population, while the segments show the uncertainties in a one standard deviation range from the mean value. (For interpretation of the references to colour in this figure legend, the reader is referred to the web version of this article.)

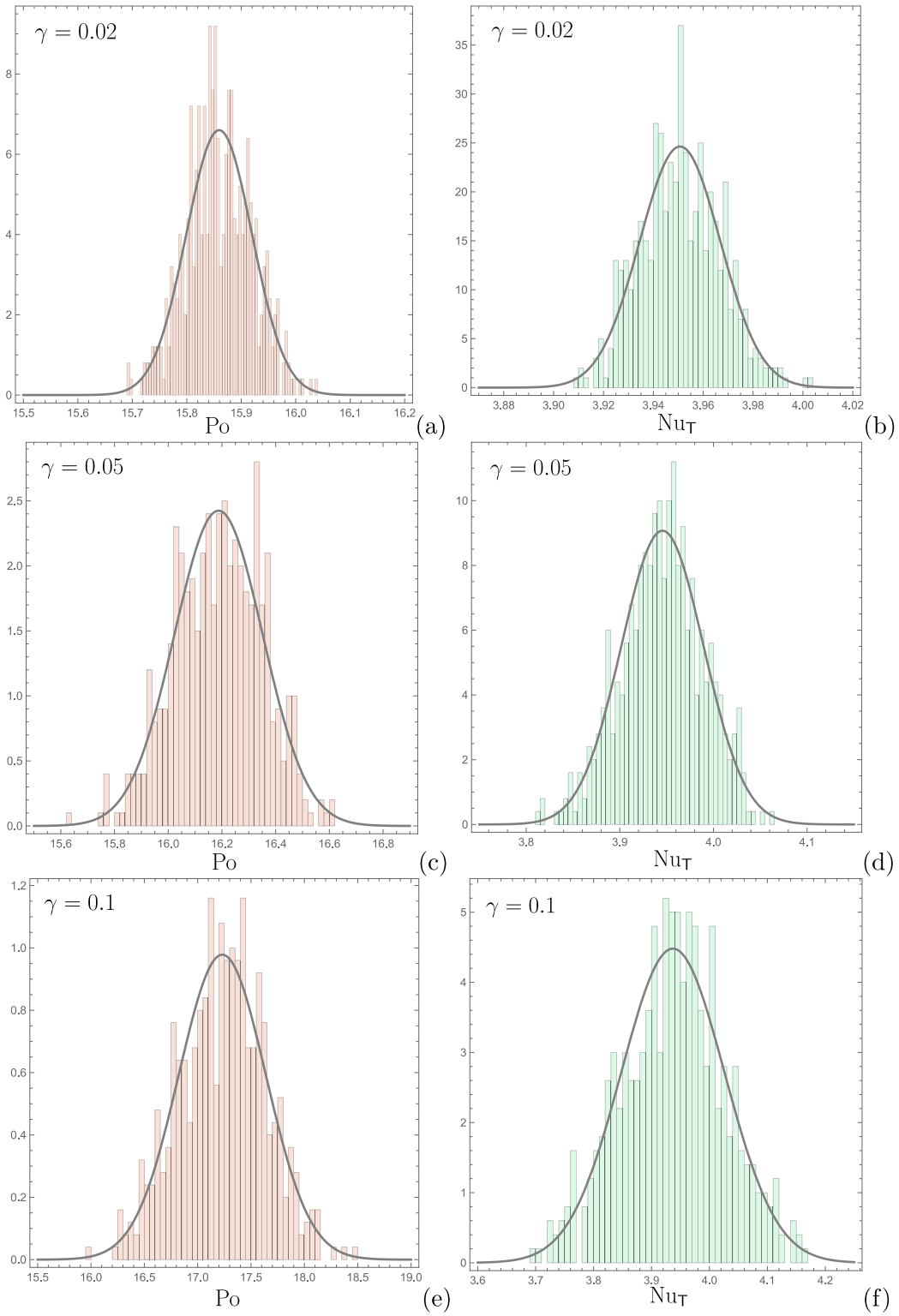

Fig. 6. Probability density plots with the actual data for Po and Nu_T for $\gamma = 0.02$ (a, b), $\gamma = 0.05$ (c, d) and $\gamma = 0.1$ (e,f). In each frame, the grey line shows the normal distribution with the same mean value and standard deviation of the data.

the local momentum balance equation, which is independent of Br, with no-slip boundary conditions. Furthermore, Nu_T is obtained by assigning a precise Brinkman number, namely $Br = Br_T$. On the other hand, Nu_{H1} and Nu_{H2} depend on the value of the Brinkman number, exactly as it happens in the case of the smooth semicircular duct (see Table 2)

Fig. 4 shows the effect of roughness on the Poiseuille number, Po, and on the Nusselt number for the T boundary condition, Nu_T. In fact, Fig. 4(b) reveals that there is no statistically relevant influence of roughness on Nu_T, at least as far as $\gamma \leq 0.1$, if not for a tendency to increasing uncertainty of the data as γ increases. Anyway, the relative uncertainty is approximately 2.3% at its largest (for $\gamma = 0.1$). On the other hand, Fig. 4(a) shows that Po increases with γ. For this parameter, the relative uncertainty is, in every case, lower than approximately 2.4%. The roughness-induced increase of Po is caused by the gradually increasing hydraulic resistance when the average length of surface spikes over the semicircular boundary becomes larger and larger. In dimensional terms, this effect corresponds to a gradually increasing value of $\mathrm{d}p/\mathrm{d}z$ for a given u_m, as one can easily infer from Eq. (9).

Fig. 5 displays the mean values and standard deviations for the Nusselt number versus γ relative to the boundary conditions H1 and H2. In this figure, frames (a) to (d) address increasing values of the Brinkman number from 0 to 1. An evident effect of the raising importance of the viscous dissipation effect is that it triggers an effect of the growing value of γ. In particular, with $Br = 0$ (negligible viscous dissipation) and $Br = 0.1$, namely for the plots shown in Figs. 5(a) and 5(b), the increasing roughness does not have a statistically significant effect on Nu for both H1 and H2 conditions. On the other hand, such an effect emerges for $Br = 0.5$ and $Br = 1$, in Figs. 5(c) and 5(d), as an increasing γ determines a weak, though indisputable, decrease in the Nusselt number in the two cases H1 and H2. The Nusselt number for the H1 condition turns out to be greater than that for the H2 condition, even though the relatively large dispersion of the data may determine a statistically relevant overlapping especially at larger values of γ and Br. This special interplay between wall roughness and viscous dissipation effect is physically grounded. In fact, for a fixed value of Br, viscous heating is enhanced by a larger roughness as an increase in γ means larger local values of the source term $2\,\mathrm{Po}^2\mathrm{Br}\,|\nabla^* u^*|^2$ in the energy balance Eq. (13), as induced both by the larger value of Po and by the typically larger local values of the gradient of u^*. The latter feature is an expected consequence of the spikes and irregularities of the roughly semicircular part of the microchannel boundary.

In Figs. 4 and 5, we explored the range $0 < \gamma \leq 0.1$. In fact, there is a reasonable upper limit to γ above which roughness effects shift to shape variability, meaning that the original smooth semicircular shape becomes completely lost. This feature is made evident by inspecting how rapidly the standard deviation of Po or Nu increases with γ, thus making the confidence interval around the mean value significantly large. There are also limitations in the random generation of the roughness geometry when γ becomes too large creating unrealistic patterns and topological oddness.

If we compare the results reported in Figs. 4 and 5 with those presented in Barletta et al. [26], we recognize that the main qualitative discrepancy emerges from the effects of the surface roughness on the parameter Nu_T. In fact, Barletta et al. [26] found that, in a circular rough microchannel, Nu_T displays a marked decrease with the roughness parameter. The main reason for the discrepancy with the trend shown in Fig. 4(b) is that the heat exchange surface (the diametrical side of the channel) is smooth in the present study, while it is affected by roughness in Barletta et al. [26]. We emphasize that, in the latter paper, a microduct with a nominally circular cross-section is studied where the whole side boundary is considered as rough and subject to heat transfer. Another correlated aspect of the comparison is that the effects of roughness on the parameters Nu_{H1} and Nu_{H2} are evident in Fig. 5, but they are definitely smaller than those found by Barletta et al. [26]. Furthermore, Nu_{H1} and Nu_{H2} are affected by the surface roughness, according to Fig. 5, only if viscous dissipation is taken into account and if it is sufficiently intense. On the other hand, roughness effects on Nu_{H1} and Nu_{H2} are found in Barletta et al. [26] also when $Br \to 0$. Thus, we may conclude that the effects of surface roughness, at the microchannel boundary, on the heat transfer rate are more relevant when the surface from which heat is actually transferred is rough.

A closer view into the statistical distribution of data for the Poiseuille number and the Nusselt number with the T boundary condition is provided in Fig. 6. In this figure, the probability density distributions for the 500 microchannels populations are displayed via histograms compared with the normal distributions having the same mean value and standard deviation of the actual data. The different frames correspond to different values of the roughness parameter γ, namely: 0.02 (frames a and b), 0.05 (frames c and d) and 0.1 (frames e and f). Fig. 6 suggests that the normal distribution represents a reasonable model for the computed data even if larger populations would be needed to attain a visually satisfactory comparison. We stress that 500 elements in each population is a statistically reliable target which, besides, shows up acceptable computational times for the finite-element solution procedure.

The statistics of data regarding the Nusselt number with H1 or H2 boundary conditions can be also illustrated through the relative uncertainty, defined as the ratio between the standard deviation δNu and the mean value Nu, expressed in percent. In fact, Fig. 7 shows the trends of $\delta\mathrm{Nu}/\mathrm{Nu}$ versus γ with $\mathrm{Br} = 0, 0.1, 0.5, 1$ for either H1 (blue circles) or H2 (red triangles) conditions. Such trends are somewhat irregular reflecting the imperfect agreement between the actual distribution of data and the normal distribution. As already pointed out while commenting on Fig. 6, this effect is a consequence of the finite, though large, number of elements in each statistical population. On one hand, the general trend is a relative uncertainty $\delta\mathrm{Nu}/\mathrm{Nu}$ increasing with γ, with the data for the H2 case being slightly more uncertain than those for the H1 case. On the other hand, the maximum $\delta\mathrm{Nu}/\mathrm{Nu}$ shown in Fig. 7 is a bit larger than 5% and it is displayed for $Br = 0$.

Viscous dissipation may have significant effects due to the microscale of the flow [15]. The analysis carried out in this paper demonstrated that this effect is an undesirable phenomenon as its consequence, for a fixed heat flux q_w, is a gradual increase of the temperature difference driving the wall heat transfer. This finding has an impact on the design of micro heat sinks for the electronic cooling, where the working fluid and the flow rate have to be chosen properly in order to minimize the effect. Moreover, we have shown that, independently of the type of boundary conditions, the effect of surface roughness on heat transfer mainly influences the dispersion of data over the statistical sample, while the mean value remains substantially unaltered. A visible reduction in the mean value of heat transfer rate (nondimensionally described by Nu) is obtained only when the effect of viscous dissipation becomes strong enough (i.e., when Br becomes large enough). Thus, one has an interplay between the effects of viscous dissipation and surface roughness where the latter tends to enhance the former. Furthermore, a quantification of the effect of roughness is provided by Fig. 5 where the change of Nu, namely the dimensionless heat transfer rate, is displayed versus the roughness parameter γ. Mapping such data into their dimensional counterparts for design purposes is straightforward when specific geometric and flow parameters are given.

6. Conclusions

A numerical analysis of the laminar forced convection in semicircular microchannels has been carried out in order to gain information on the thermal characteristics of heat sinks designed for cooling a heated metal plate. While the metal plate, corresponding to the diametrical boundary of the microchannel has been supposed to be polished and, hence, perfectly smooth, the semicircular boundary has been considered as having a significant roughness.

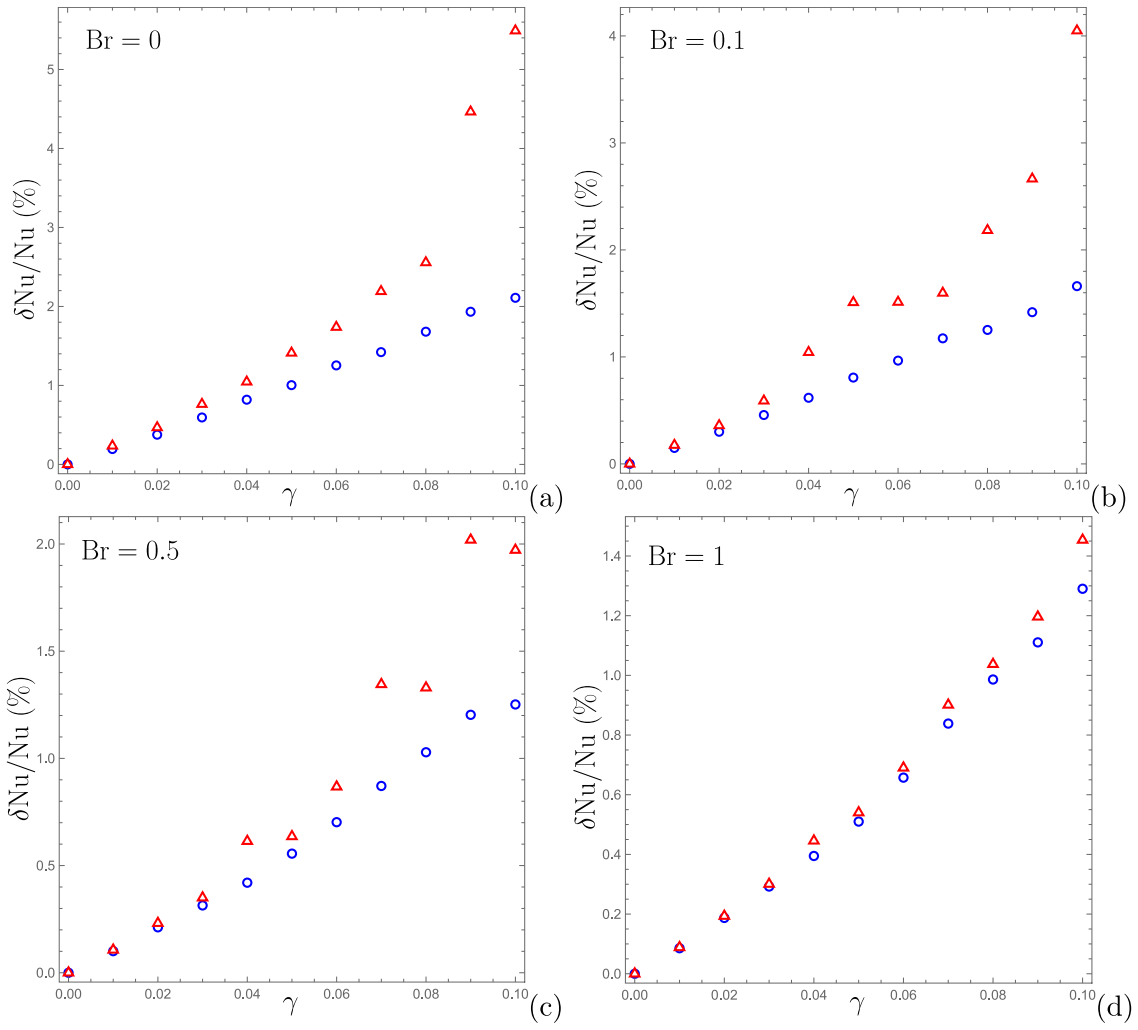

Fig. 7. Relative uncertainty for Nu versus γ with the H1 (blue ∘) and H2 (red △) boundary conditions with different Brinkman numbers. (For interpretation of the references to colour in this figure legend, the reader is referred to the web version of this article.)

The numerical solution of the local momentum balance and the local energy balance equations has been obtained for each randomly generated domain by employing the finite element method developed within the software environment *Wolfram 14* [29]. The main results obtained in our study can be summarized as follows:

- The flow mechanical resistance, described by the Poiseuille number Po, turns out to increase with the wall roughness parameter γ displaying an increasing statistical dispersion of the data and, hence, an increasing standard deviation, as the roughness increases.
- The Nusselt number for the special T boundary condition turned out to be unaffected by the wall roughness even though its standard deviation increases with γ.
- The Nusselt number Nu for the cases H1 and H2 is independent of γ when the viscous dissipation effect is neglected (Br → 0), though Nu_{H1} is generally larger than Nu_{H2}. The latter is a typical feature of laminar forced convection flows [28].
- When viscous dissipation is non-negligible, then both Nu_{H1} and Nu_{H2} tend to decrease with γ, showing up a significant increase of the standard deviation which, in some cases, tends to yield a partial overlap of the confidence intervals for these parameters.

By comparing the results of the present analysis with those reported in a similar study relative to a microduct with a nominally circular cross-section [26], we have concluded that the effects of roughness are definitely minor when the heat transfer is from a perfectly smooth part of the boundary, even if the rest of the boundary is affected by roughness.

In our analysis, the special case of the smooth semicircular duct ($\gamma \to 0$) has been considered as a benchmark case which is well-known from the existing literature only with reference to the Poiseuille number [31,34]. On the other hand, the values of the Nusselt number have been obtained numerically in this paper, due to the peculiar assignment of the thermal boundary conditions which differs from those typically considered in the literature.

We emphasize that the temperature boundary condition of thermal insulation at the nominally semicircular boundary can be improved to a more realistic one. A possible candidate is a third-kind boundary condition allowing for a finite thermal resistance of the slab where the semicircular passages are etched. A significant improvement of this study can be achieved by extending the analysis to a three-dimensional model where the roughness is not streamwise invariant. We mention that, although a three-dimensional study is significantly more realistic, its implementation is by and large more demanding in terms of computational time and in terms of number of governing parameters. The Reynolds number and the Prandtl number would enter the governing equations making any attempt to generality in the discussion of the results a considerably difficult, though challenging, task.

CRediT authorship contribution statement

A. Barletta: Writing – review & editing, Writing – original draft, Validation, Methodology, Investigation, Funding acquisition, Formal analysis, Conceptualization. **M. Celli:** Writing – review & editing, Writing – original draft, Validation, Methodology, Investigation, Funding acquisition, Formal analysis, Conceptualization. **P.V. Brandão:** Writing – review & editing, Writing – original draft, Validation, Methodology, Investigation, Funding acquisition, Formal analysis, Conceptualization.

Declaration of competing interest

The authors declare the following financial interests/personal relationships which may be considered as potential competing interests: all authors declare that they have no known competing financial interests or personal relationships that could have appeared to influence the work reported in this paper.

Acknowledgements

The work by Antonio Barletta, Michele Celli and Pedro Vayssière Brandão was supported by Alma Mater Studiorum Università di Bologna, grant number RFO-2024.

Data availability

No data was used for the research described in the article.

References

[1] M.G. Khan, A. Fartaj, A review on microchannel heat exchangers and potential applications, Int. J. Energy Res. 35 (2011) 553–582.
[2] S.G. Kandlikar, History, advances, and challenges in liquid flow and flow boiling heat transfer in microchannels: A critical review, ASME J. Heat Transf. 134 (2012) 034001.
[3] O.K. Siddiqui, S.M. Zubair, Efficient energy utilization through proper design of microchannel heat exchanger manifolds: A comprehensive review, Renew. Sustain. Energy Rev. 74 (2017) 969–1002.
[4] N. Gilmore, V. Timchenko, C. Menictas, Microchannel cooling of concentrator photovoltaics: A review, Renew. Sustain. Energy Rev. 90 (2018) 1041–1059.
[5] D. Deng, L. Zeng, W. Sun, A review on flow boiling enhancement and fabrication of enhanced microchannels of microchannel heat sinks, Int. J. Heat Mass Transfer 175 (2021) 121332.
[6] M. Harris, H. Wu, W. Zhang, A. Angelopoulou, Overview of recent trends in microchannels for heat transfer and thermal management applications, Chem. Eng. Process. – Process. Intensif. 181 (2022) 109155.
[7] B. Heidarshenas, A. El-Shafay, S.M. Sajadi, Y. Yuan, Enhancing efficiency in microscale systems with microchannels: A review, J. Therm. Anal. Calorim. (2024) 1–26.
[8] B. Dash, J. Nanda, S.K. Rout, The role of microchannel geometry selection on heat transfer enhancement in heat sinks: A review, Heat Transf. 51 (2022) 1406–1424.
[9] Z.-Q. Yu, M.-T. Li, B.-Y. Cao, A comprehensive review on microchannel heat sinks for electronics cooling, Int. J. Extrem. Manuf. 6 (2024) 022005.
[10] W. Dong, X. Zhang, B. Liu, B. Wang, Y. Fang, Research progress on passive enhanced heat transfer technology in microchannel heat sink, Int. J. Heat Mass Transfer 220 (2024) 125001.
[11] B. Xu, K.T. Ooi, C. Mavriplis, M.E. Zaghloul, Evaluation of viscous dissipation in liquid flow in microchannels, J. Micromech. Microeng. 13 (2002) 53.
[12] J. Koo, C. Kleinstreuer, Viscous dissipation effects in microtubes and microchannels, Int. J. Heat Mass Transfer 47 (2004) 3159–3169.
[13] G. Croce, P. D'Agaro, Numerical analysis of roughness effect on microtube heat transfer, Superlattices Microstruct. 35 (2004) 601–616.
[14] G. Croce, P. D'Agaro, Numerical simulation of roughness effect on microchannel heat transfer and pressure drop in laminar flow, J. Phys. D: Appl. Phys. 38 (2005) 1518–1530.
[15] H. Bruus, Theoretical Microfluidics, Oxford University Press, 2007.
[16] G. Croce, P. D'Agaro, C. Nonino, Three-dimensional roughness effect on microchannel heat transfer and pressure drop, Int. J. Heat Mass Transfer 50 (2007) 5249–5259.
[17] J. Van Rij, T. Ameel, T. Harman, The effect of viscous dissipation and rarefaction on rectangular microchannel convective heat transfer, Int. J. Therm. Sci. 48 (2009) 271–281.
[18] M.B. Turgay, A.G. Yazicioglu, Effect of surface roughness in parallel-plate microchannels on heat transfer, Numer. Heat Transf. Part A: Appl. 56 (2009) 497–514.
[19] C. Nonino, S. Del Giudice, S. Savino, Temperature-dependent viscosity and viscous dissipation effects in microchannel flows with uniform wall heat flux, Heat Transf. Eng. 31 (2010) 682–691.
[20] N. Pelević, T.H. van der Meer, Heat transfer and pressure drop in microchannels with random roughness, Int. J. Therm. Sci. 99 (2016) 125–135.
[21] S. Mukherjee, P. Biswal, S. Chakraborty, S. DasGupta, Effects of viscous dissipation during forced convection of power-law fluids in microchannels, Int. Commun. Heat Mass Transfer 89 (2017) 83–90.
[22] D. Jing, Y. Pan, X. Wang, Joule heating, viscous dissipation and convective heat transfer of pressure-driven flow in a microchannel with surface charge-dependent slip, Int. J. Heat Mass Transfer 108 (2017) 1305–1313.
[23] H. Lu, M. Xu, L. Gong, X. Duan, J.C. Chai, Effects of surface roughness in microchannel with passive heat transfer enhancement structures, Int. J. Heat Mass Transfer 148 (2020) 119070.
[24] A. Barletta, Fully developed laminar forced convection in circular ducts for power-law fluids with viscous dissipation, Int. J. Heat Mass Transfer 40 (1996) 15–26.
[25] H. Wang, Y. Wang, Influence of three-dimensional wall roughness on the laminar flow in microtube, Int. J. Heat Fluid Flow 28 (2007) 220–228.
[26] A. Barletta, M. Celli, L.A. Sphaier, P.V. Brandão, S. Lazzari, E. Ghedini, Shape uncertainty analysis of laminar forced convection in a round microchannel with viscous dissipation, Appl. Therm. Eng. 265 (2025) 125536.
[27] L.A. Sphaier, A. Barletta, M. Celli, P.V. Brandão, E. Ghedini, Laminar forced convection in circular microchannels with slip-flow: Analysis of randomly distributed roughness, Int. Commun. Heat Mass Transfer 162 (2025) 108615.
[28] R.K. Shah, A.L. London, Laminar flow forced convection in ducts, in: Advances in Heat Transfer, Academic Press, 1978.
[29] Wolfram Research, Inc., Mathematica, Version 14.2, Champaign, IL, 2024, https://www.wolfram.com/mathematica.
[30] R.M. Manglik, A.E. Bergles, Laminar flow heat transfer in a semi-circular tube with uniform wall temperature, Int. J. Heat Mass Transfer 31 (1988) 625–636.
[31] E.M. Languri, K. Hooman, Slip flow forced convection in a microchannel with semi-circular cross-section, Int. Commun. Heat Mass Transfer 38 (2011) 139–143.
[32] R.S. Alassar, Fully developed forced convection through semicircular ducts, J. Thermophys. Heat Transfer 28 (2014) 560–565.
[33] S. Mukherjee, A.K. Gupta, R.P. Chhabra, Laminar forced convection in power-law and Bingham plastic fluids in ducts of semi-circular and other cross-sections, Int. J. Heat Mass Transfer 104 (2017) 112–141.
[34] S. Kyritsi-Yiallourou, G.C. Georgiou, Newtonian Poiseuille flow in ducts of annular-sector cross-sections with Navier slip, Eur. J. Mech. B Fluids 72 (2018) 87–102.